Simulation of Strain in ReBCO Tapes Under Combined Helical-Hard-Way Bending and Critical Current Measurements

Hamed Milanchian, Mohsen Haajari, Mika Lyly, and Tiina Salmi

***Abstract*—In this study, we investigate the mechanical behavior of high-temperature superconducting tapes under combined helical-hard-way bending load. The combined bending scenario is related to a helically wound solenoid where hard-way bending arises due to the connection of the tapes to the current terminals. Similar phenomena can also occur in double pancake coils due to the layer transitions. We have sought simulation methods to assess the associated mechanical strain that may lead to critical current degradation. Experimental measurements involve winding SuperOx 2G ReBCO tapes around formers with varying radii and lead angles to assess the critical current degradation resulting from combined helical-hard-way. The experimental procedure, results, and the utilized ANSYS finite element modeling approaches are presented. The strain distribution across different modeling assumptions is compared, including 2D and 3D tape models, homogenized tape material properties, and simulations accounting all tape layers individually. We evaluated the pros and cons of the presented approaches which are expected to be useful for future detailed analysis of such scenarios.**

***Index Terms*—ReBCO tapes, YBCO, critical current, solenoids, mechanical analysis, bending, FEM.**

I. Introduction

YBCO-BASED 2G ReBCO tapes demonstrate potential for high-field electromagnet applications. Their performance surpasses traditional low-temperature superconductors [1]. However, during the winding process and also in operational environments, especially in high-field, high-current density applications, these ReBCO tapes are subjected to mechanical strains and magnetic fields, which can adversely affect their critical current (I_c) performance. To thoroughly assess the accumulated degradation of I_c performance, it is crucial to evaluate the strain during winding, serving as a baseline for subsequent electromagnetic and other loadings. ReBCO tapes, depending on their application, may encounter various bending scenarios, including easy-way bending, helical bending, hard-way bending, or a combination of loads with tension during winding. This paper focuses on strain simulations under a combined bending condition.

Several studies have investigated the behavior of ReBCO tapes under various bending scenarios, employing numerical, experimental, and analytical approaches. In a study focusing on the pure easy-way bending case of ReBCO tapes, numerical investigation of strain was conducted and compared to analytical approaches, considering parameters such as width and thickness of constituting layers [2]. Another investigation focused on SuNAM tapes, which were subjected to double bending on both sides at room temperature and different bending diameters prior to cooling to cryogenic temperatures [3]. Numerous studies have also gone through helical bending especially for CORC cable and Canted-Cosine-Theta (CCT) dipole applications. The strain in the REBCO layer was numerically determined using the constant-perimeter geometry method, suitable for applications such as helical winding and CCT dipoles and quadrupoles [4]. Another study utilized ABAQUS software to assess the mechanical behavior of CORC cable winding and its impact on I_c degradation, specifically studying the helix angle of the cable and the substrate thickness of the tape to determine the ideal winding radius [5]. For power cable HTS applications, a 3D ANSYS finite element model (FEM) was introduced to study the strain behavior of 2G Superpower tapes under axial tensile and twisting loads during helical winding, combined with external tensile and bending loads [6]. Regarding pure hard-way bending in coil applications, an analytical approach is introduced to investigate hard-way bending in stacked cables, where the absence of gaps between turns induces hard-way bends. To address this issue, the authors propose a geometrical model that seeks to minimize the occurrence of hard-way bending in the design of 3D coils [7]. Some studies have also investigated combined loads. For example, using COMSOL models and varying parameters such as the thickness of Hastelloy and copper layers, as well as the width of the tape, a study explored the combined effects of tension and torsion loads on inducing axial strain [8]. In recent studies, specific bending scenarios have been explored, such as the effect of width-wise bending on the permanent I_c degradation of ReBCO tapes [9].

However, in coils, some other critical sections with combined bending can be found. For example, in solenoids or pancake coils, where tapes exit the former to the current terminals combined helical-hard-way bending loads can be induced. This study aims to investigate the effect of combined helical-hard-way bending loads on these coils. For this purpose, a combined helical-hard-way bending scenario is simulated with a FEM

Manuscript received 26 September 2023; revised 18 December 2023; accepted 22 January 2024. Date of publication 26 January 2024; date of current version 12 February 2024. This work was supported in part by Superconducting Magnets Beyond 20 T (Super20 T), Academy of Finland, under Grant 324887, and in part by the Business Finland Co-Innovation Project SMARAGDI under Grant 3972/31/2019. *(Corresponding author: Hamed Milanchian.)*

Hamed Milanchian, Mohsen Haajari, and Tiina Salmi are with the Department of Electrical Engineering, Tampere University, 33720 Tampere, Finland (e-mail: hamed.milanchian@tuni.fi).

Mika Lyly was with the Tampere University, 33100 Tampere, Finland. He is now with the Quanscient, 33100 Tampere, Finland.

Color versions of one or more figures in this article are available at https://doi.org/10.1109/TASC.2024.3358764.

Digital Object Identifier 10.1109/TASC.2024.3358764

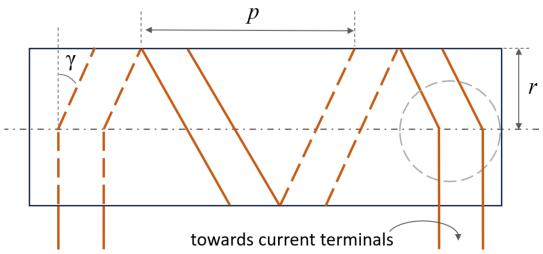

Fig. 1. Tape schematically wound helically around a former with highlighted combined bending section.

software with a large-deformation analysis and taking into the account the impact of distinct material layers. Additionally, I_c measurements on SuperOx tapes have been performed. The primary objective is to develop methods for simulating combined bending scenarios that are applicable to specific types of solenoids.

II. Combined Bending Scenario

The combined bending scenario considered in this study comes from a small helically wound solenoid designed and constructed at Tampere University. This small coil served as an experimental platform for validating various simulation tools. Recognizing the mechanical complexities in such coils, a method was sought to assess the risks associated with these combined bends. The bending scenario arises when the first (or last) helical turn of the wound tape is leaving the former to be connected to the current terminals. Potentially a hard-way bending component is induced with respect to the helix lead angle. In a former with a radius of r (see Fig. 1), a helix is formed with a lead angle (γ). The pitch of the helix (p) is also indicated in the figure. The lead angle is computed as: $\gamma = \arctan\left(\frac{p}{2\pi r}\right)$. The combined bending area is highlighted with a circle in Fig. 1. For this study, formers near the critical bending radius of the ReBCO tape are considered. The critical diameter of SuperOx ReBCO tape with a substrate thickness in the range of 60 μm is reported as 15 mm, indicating that it can handle easy-way bending without degradation up to a 7.5 mm radius former [10]. As the study involves combined helical-hard-way bending loads, radii from 15 mm to 5 mm are investigated in this work. Considering the 4 mm width of the SuperOx tape, a minimum pitch of 5 mm is set to avoid stacking tapes, and pitches of 6 mm and 7 mm are also considered. Therefore, the calculated lead angles range between 3–9 degrees. Further details about the formers used in this work are explained in Section III-B.

III. Experimental Procedure

The experiments are conducted at the Tampere University Cryolab. For these experiments, the strategy involves measuring the tape's I_c in its unwound (no-loading) state. The tape is then wound around a cylinder, and its I_c is measured again to assess any degradation due to winding-induced bending.

A. ReBCO Tape: SuperOx

For the I_c measurements, SuperOx 2G ReBCO tapes are utilized. The manufacturer reports a minimum I_c of 136 A at 77 K for the spool containing a 50 m length of tape and recommends a bending radius no smaller than 7.5 mm. The tape is insulated on both sides with varnish polyimide and consists of copper, Hastelloy C276, YBCO, and silver. The YBCO layer faces outward when the tape is drawn from the spool and it faces to outer radius also during measurements and simulations. The width of the tape is 4 ± 0.13 mm, and the layer thicknesses reported by the manufacturer are detailed in Table I. A total of four samples, each around 60 cm in length, are cut and employed for the tests.

TABLE I
Layer Thicknesses in SuperOx ReBCO tape [10] and Elastic Material Properties Used for the Tape Model [1]

	thickness [μm]	α_{th} [K^{-1} $\times 10^{-6}$]	E [GPa]	ν
copper	20 ± 4	17.7	80	0.338
Hastelloy	63 ± 3	13.4	200	0.307
YBCO	2.4	11	157	0.3

Fig. 2. 3D printed formers for I_c testing.

TABLE II
Printed Formers Specifications

Formers	Radius [mm]	Pitch [mm]	turns	bending length [cm]	lead angle [°]
F^5_{15}	15	5	2.5	23.60	3.04
F^7_{15}	15	7	2.5	23.63	4.25
F^5_{10}	10	5	2.5	15.76	4.55
$F^5_{7.5}$	7.5	5	3.5	16.59	6.06
$F^6_{7.5}$	7.5	6	3.5	16.63	7.26
F^5_5	5	5	4.5	14.32	9.04

B. Formers

The tape is wound around a cylindrical former, in a helical configuration. Formers are created using 3D printing with Tough 1500 material from Formlabs. Six different formers are used in total. To ensure reliable results, multiple turns are included in the formers, aiming for a bending length of over 10 cm. Images of these 3D-printed formers can be seen in Fig. 2. The specifications of the individual formers are summarized in Table II. Formers are labeled as F^p_r, where r represents the bending radius and p denotes the pitch of the helix.

C. Procedure and Tests

The sample holder is made of Bakelite. Two copper terminals, each approximately 4 cm in length, have been securely screwed onto it (shown in Fig. 4). Prior to the test, preparation is needed for each sample. First, the insulation is removed from the ends and voltage measuring points using sodium hydroxide solution. Formers are positioned on the sample holder and screws are

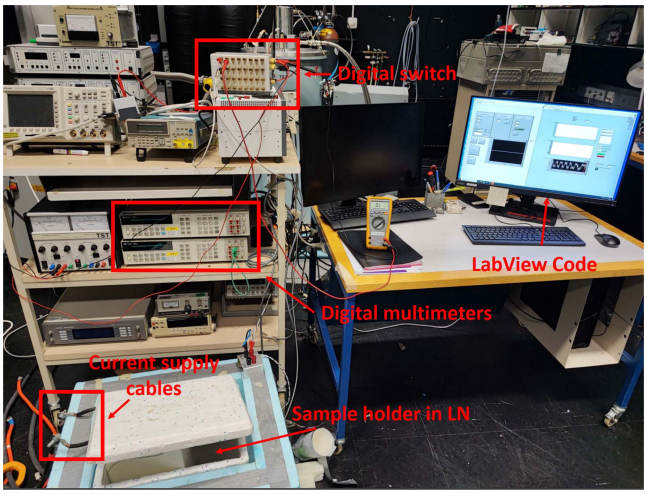

Fig. 3. Test environment.

Fig. 4. F_5^5 former and sample holder in the cooling box during the short circuit test.

partially tightened. The sample is then wound around the former, and soldered to the copper terminals, after which the former is completely tightened and secured. The experimental setup includes a power supply capable of delivering up to 200 A, a digital multimeter for measuring voltage, and a switch for quench detection and channel switching, powered by a 5 V supply. The input current is measured using hall effect current transducer. All these steps are performed in the test environment shown in Fig. 3. The sample holder is placed inside a cooling box and terminals are connected to the current supply. Initially, the whole setup, along with the LabVIEW software code, is tested through a short circuit test. The voltage outputs, current supply, and quench detection/protection code are all verified. Fig. 4 displays the sample wound around the F_5^5 former, and being tested in a short circuit test. The quench detection/protection code operates based on a critical voltage value, which is initially set according to the length of the tape. Following this, liquid nitrogen is used to cool the sample to 77 K.

IV. Experimental Results

The measured voltage and current data are explored through a power law relationship to calculate the I_c for each respective sample. The voltage-current relationship is fitted using the equation:

$$V = V_c \left(\frac{I}{I_c}\right)^n \tag{1}$$

During the current ramp-up phase, the critical voltage (V_c), I_c, and the n value are determined using a non-linear least squares fitting method. The reference (initial) critical current values for the samples, represented as I_{c0}, are measured to be 157 $\pm$ 3 A. The exact measured I_{c0} values for each sample are considered when computing the normalized I_c in bending cases (Table III). Later, samples wound around formers undergo the same procedure, and the relevant I_c is measured for each case. These results can be found in Table III. Tape sample 1 was initially tested with formers F_{15}^5, F_{15}^7, and F_{10}^5, showing no degradation. As these measurements provided consistent results, there was no need for repetition, and confidence was established in the safe use of radii ranging from 15 to 10 mm, corresponding to lead angles of 3 to 4.5 degrees. An extreme case involving F_5^5 was then examined with tape sample 1, resulting in an observable degradation. Due to the uncertainty regarding the reversibility of this degradation, a new test sample (test sample 2) was introduced. This sample was exclusively used with the F_5^5 former to repeat the observed degradation. Notably, test sample 2 exhibited an 85% reduction in I_c, suggesting irreversible degradation. Subsequently, test sample 3 assesses formers with a radius of 7.5 mm and lead angles of 6 to 7.3 degrees. To further ensure the reliability of results for 7.5 mm formers, test sample 4 was employed. Test sample 4 was used exclusively with $F_{7.5}^5$ and the results obtained with test sample 3 were repeated. Throughout the testing and measurements, the selection of test samples was to avoid irreversible reductions in I_c. Additionally, formers with critical radii underwent multiple tests to reproduce and thereby validate the results. The impact of combined bending radius and lead angle change on I_c reduction is graphically represented in Fig. 5 .

TABLE III
I_c of Samples Wound Around Different Formers

Sample	F	V_c [μV]	I_c [A]	I_c/I_{c0}
1	F_{15}^5	182.79	158.61	1.02
1	F_{15}^7	185.93	157.04	1.01
1	F_{10}^5	188.70	155.65	1.00
1	F_5^5	169.39	36.31	0.23
2	F_5^5	225.47	22.94	0.15
3	$F_{7.5}^5$	144.88	157.30	0.98
3	$F_{7.5}^6$	142.85	158.57	0.99
4	$F_{7.5}^5$	146.54	156.64	1.00

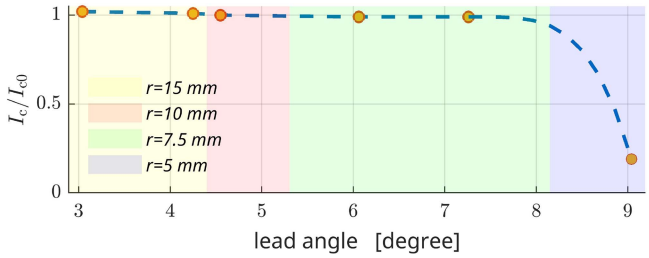

Fig. 5. I_c drop by bending radius and lead angle of the formers.

V. Tape Mechanical Modeling With ANSYS

A. Geometry of the Simulation

The simulated tape consists of one quarter of a turn around the former and the section that the tape exits towards the current terminal. The starting point for the simulation is a straight tape.

TABLE IV
SUMMARY OF ANSYS SIMULATIONS

Case	Sim.	Initial state	End state	Load(s)
0	2D	straight	easy-way bent	easy-way bending
1	3D	straight	easy-way bent	easy-way bending
2	3D	easy-way bent	final	combined-bending+cool-down

The winding procedure is simulated in two stages. In the first stage, the tape end towards the current terminal is fixed and a displacement and rotation is applied to the other end to apply easy-way bending corresponding to the former radius. In the second stage, the bent end of the tape is displaced and rotated to obtain the desired helical angle and to complete the combined helical-hard-way bending load. To naturally bend the end of the tape in both stages, the displacement and rotation are achieved by computing trajectories. Subsequently, the tape is cooled to 77 K.

The resulting strain are computed under large-deformation assumptions. The electromagnetic load during the I_c measurement is not simulated. The lengths of the tape pieces are selected to obtain sufficient numerical stability: Tape pieces longer than one quarter of a turn and exiting section longer than 5 mm appeared to induce undesired buckling issues.

Simulating this geometry is challenging, and no references in previous works were found to assess this specific type of bending. The closest one was the simulation of helical bending in CORC cables, where the tape was initially aligned with the former and then the former was rotated [6][11].

B. Homogenization of Material Properties

To address the challenge of long computation time related to the thin material layers, two approaches are compared: a 2D model including all material layers individually and a 3D model with homogenized material properties. The homogenized material properties for the 3D model are calculated by:

$$\bar{F} = \frac{\sum F_i \, t_i}{t} \tag{2}$$

Here, $\bar{F}$ represents the homogenized material property, while F_i denotes each layer's material property. The thickness of each layer and the overall tape thickness are represented by t_i and t, respectively. Table IV summarizes the simulation cases.

C. 2D Tape Model With Individual Layers: Easy-Way Bending

The 2D model is oriented parallel to the base of the cylinder and represents the length of the tape by focusing on its side cross-section (case 0). The simulation uses a plane-strain model. A four-layered ReBCO tape is chosen, including two copper layers, Hastelloy, and YBCO layer. The negligible impact of the silver and buffer layers on the observed results is recognized, so they are omitted [1]. The elastic material properties (E, ν and α_{th}, respectively the Young's modulus, Poisson's ratio, and the coefficient of thermal expansion), and thicknesses of each layer are summarized in Table I. The bonding between the Hastelloy and the ReBCO layer (or more specifically the buffer layer) is known to be mechanically weak which leads to delamination under shear and transverse stresses [12][13]. We neglect any possible delamination occurring in our combined bending load, and consider perfectly bonded layers. The simulated tape strain and YBCO layer strain values are averaged across the tape length for the wound part around the former and are provided in Table V. As the YBCO layer faces outward, it experiences traction with an average of 0.29% strain in the case of a 5 mm bending radius after easy-way bending. The tape's strain stays below 0.02% in all bending radii.

TABLE V
TAPE AND YBCO LAYER AVERAGE AXIAL STRAIN

Formers	case 0			case 1		
	F^5_{10}	$F^5_{7.5}$	F^5_5	F^5_{10}	$F^5_{7.5}$	F^5_5
ϵ_{axial}YBCO [%]	0.147	0.196	0.291	0.154	0.203	0.293
ϵ_{axial}tape [%]	0.006	0.009	0.017	0.010	0.013	0.020

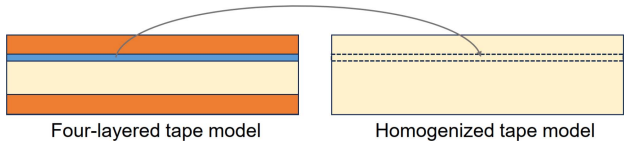

Fig. 6. YBCO layer projection from 2D model to 3D model.

D. 3D Homogenized Modeling: Comparison of 2D and 3D Case for Easy-Way Bending

In case 1, only easy-way bending simulation is performed. Given the YBCO layer's location in the layered tape, an estimated strain value for the 3D model can be attributed to the YBCO layer (Fig. 6). Based on this approach, tape axial strain and the estimated axial strain of the YBCO layer are averaged across the tape length for the wound part around the former and are provided in Table V. The easy-way bending results from the 2D detailed study and the 3D homogenized study (as shown in Table V) are compared. The YBCO layer strain estimated by the 3D study shows less than 5% difference to the 2D study, and all average tape axial strains are within 0.02% in both studies. Due to the small difference in the easy-way bending cases in both studies, we decided to use the 3D homogenized model for the rest of the simulations.

E. 3D Homogenized Modeling: Combined Helical-Hard-Way Bending + Cool-Down

To simulate the entire loading, two separate simulations (case 1 and case 2) are carried out, and their results are later combined. The deformation of the ReBCO tape with the former F^5_5 configuration in both simulations are displayed in Fig. 7. The impact of the combined helical-hard-way bending is evident from the asymmetric deformation and buckling observed. Due to the non-uniform deformation in the tape, the axial strain is expected to exhibit non-uniformity particularly across its cross-section. The axial strain results at the middle cross-section of the wound part of the tape with the F^5_5 former are shown in Fig. 8. The axial strain due to the entire loading is computed by summing the results from case 1 and case 2 simulations. A uniform axial strain (along the tape width) ranging from -0.3% to 0.3% is observed in the easy-way bending simulation. In the entire loading, all parts of the cross-section experience tensile strain, and the strain

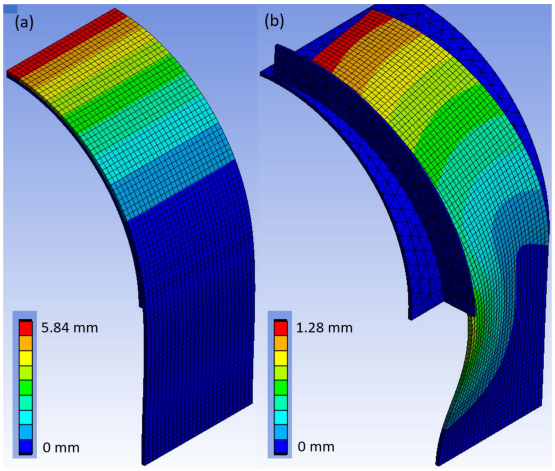

Fig. 7. ReBCO tape deformation with former F_5^5 (a) case 1 and (b) case 2.

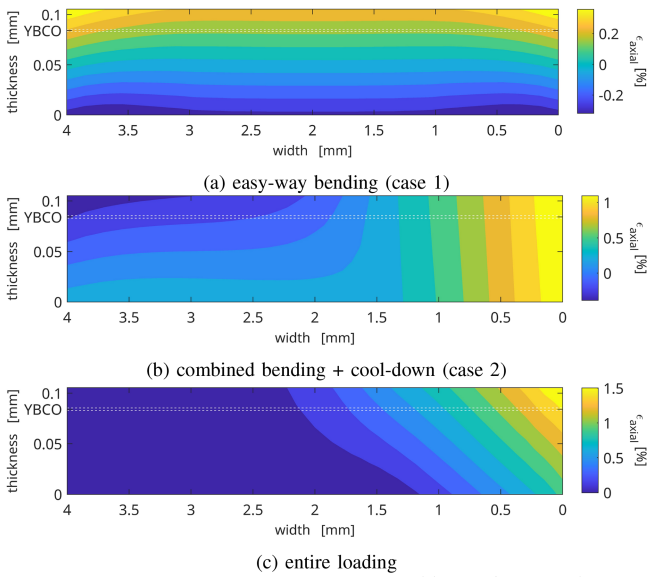

Fig. 8. Axial strain at tape cross section (middle of the wound part) with F_5^5 former.

is highly non-uniform, with the right-top part of the tape reaching locally a maximum axial strain of 1.5%.

VI. Discussion

The simulation results revealed a highly non-uniform axial strain distribution in the tape cross-section due to combined helical-hard-way bending. In an effort to establish a correlation between experimental I_c degradation and simulated axial strain, average and maximum strain values are computed. For the tape, the average and maximum values are calculated along the tape length. However, for the YBCO layer, the axial strain is first averaged within the YBCO layer before calculating the average and maximum values along the length. Fig. 9 correlates the measured I_c drop and the axial strain obtained from the related simulations. The simulated tape strain values of 0.30% to 0.34% correspond to the measured I_c degradation. For the YBCO layer, measured I_c degradation is observed within the range of 0.49%

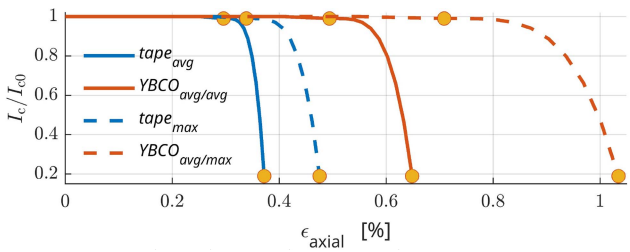

Fig. 9. Measured I_c drop with simulated axial strain in tape and YBCO layer ($YBCO_{avg/max}$ denotes the average value within the layer and then maximum value along the length).

to 0.71% simulated axial strain. Notably, if the maximum axial strain value within the YBCO layer is considered without any averaging, I_c degradation is not observed until reaching locally to 2.24% of simulated axial strain (not shown in Fig. 9).

While establishing this correlation, it is essential to recognize potential sources of error that may arise from both simulations and measurements, which can impact the accuracy of the correlation. The contraction of the holder material (Bakelite) is not accounted for in our simulations, which could lead to higher axial strains in the simulated results compared to the measurements. Moreover, tapes are manually wound without the use of machines, and the fixed point (terminal) is positioned at a distance from the former. However, in the simulations, a shorter length of tape is considered for that part. This difference could potentially lead to higher simulated axial strains in the simulation as well.

Regarding the magnetic field effect, the critical current degradation induced by the magnetic field in the solenoids was numerically estimated using an in-house COMSOL model. The simulations suggested that in solenoids with radii ranging from 10 to 5 mm, the resulting critical current change was less than 5 A. Therefore, we do not expect that the measured degradation in our study is associated with changes in the magnetic field distribution.

VII. Conclusion

This research explored the combined helical-hard-way bending scenario in ReBCO tape solenoids, focusing on its impact on critical current degradation. Critical current measurements were performed using various formers, and both 2D and 3D FEM simulations were carried out to estimate combined helical-hard-way bending as well as the cool-down. The strain distribution in the tape, after being wound around these formers, was determined, and the strain within the YBCO layer was estimated using the 3D homogenized model based on the geometric location. The difference between the 2D model including all layers and the 3D homogenized model in the easy-way bending scenario resulted in a 5% difference in axial strain. The non-uniformity of axial strain values from the 3D study presents challenges in directly correlating the simulated axial strain to measured critical current degradation.

References

[1] H. Milanchian, T. Salmi, A. Halbach, and R. Kouhia, "HTS tape mechanical behavior sensitivity on material properties and thickness of material layers," *IEEE Trans. Appl. Supercond.*, vol. 33, no. 5, Aug. 2023, Art. no. 8400605.

[2] K. Ashok, R. J. Thomas, J. P. Mathai, and A. Nijhuis, "Analytical and numerical investigations on the degradation of REBCO based superconducting tapes under bending," *IEEE Trans. Appl. Supercond.*, vol. 31, no. 7, Oct. 2021, Art. no. 8400712.

[3] D. P. Boso, M. Breschi, A. Musso, E. Pilastro, and P. L. Ribani, "Numerical investigation on the thermo-mechanical behavior of HTS tapes and experimental testing on their critical current," *IEEE Trans. Appl. Supercond.*, vol. 30, no. 4, Jun. 2020, Art. no. 8400305.

[4] X. Wang, D. Arbelaez, S. Caspi, S. O. Prestemon, G. Sabbi, and T. Shen, "Strain distribution in REBCO-coated conductors bent with the constant-perimeter geometry," *IEEE Trans. Appl. Supercond.*, vol. 27, no. 8, Dec. 2017, Art. no. 6604010.

[5] K. Wang, W. Ta, and Y. Gao, "The winding mechanical behavior of conductor on round core cables," *Physica C: Supercond. Appl.*, vol. 553, pp. 65–71, 2018.

[6] I. Das, V. Sahoo, and V. Rao, "Structural analysis of 2G HTS tapes under different loading conditions for HTS power cable using finite element modeling," *Physica C: Supercond. Appl.*, 2020, Art. no. 1353771.

[7] T. Nes, G. de Rijk, A. Kario, and H. ten Kate, "Differential geometry method for minimum hard-way bending 3D design of coils with REBCO tape conductor," *Supercond. Sci. Technol.*, vol. 35, no. 10, 2022, Art. no. 105011.

[8] A. Kb, R. J. Thomas, J. P. Mathai, and A. Nijhuis, "Influence of combined tension and torsion on the performance of REBCO superconducting tapes," *IEEE Trans. Appl. Supercond.*, vol. 33, no. 3, Apr. 2023, Art. no. 7500211.

[9] M. B. de Leon, A. R. Nisay, M. A. Diaz, and H.-S. Shin, "Widthwise bending-induced response of critical current in REBCO tapes," *IEEE Trans. Appl. Supercond.*, vol. 33, no. 5, Aug. 2023, Art. no. 8401105.

[10] A. Molodyk et al., "Development and large volume production of extremely high current density $YBa_2Cu_3O_7$ superconducting wires for fusion," *Sci. Rep.*, vol. 11, no. 1, 2021, Art. no. 2084.

[11] F. Pierro et al., "Finite-element analysis of the strain distribution due to bending in a REBCO coated conductor for canted cosine theta dipole magnet applications," *IEEE Trans. Appl. Supercond.*, vol. 29, no. 5, Aug. 2019, Art. no. 4600705.

[12] L. Liu, Y. Zhu, X. Yang, T. Qiu, and Y. Zhao, "Delamination properties of YBCO tapes under shear stress along the width direction," *IEEE Trans. Appl. Supercond.*, vol. 26, no. 6, Sep. 2016, Art. no. 6603406.

[13] Z. Zhao, P. Moore, and L. Chiesa, "Structural finite element analysis of REBCO tape delamination with solid-shell element under various loads," *IOP Conf. Series: Mater. Sci. Eng.*, vol. 1241, 2022, Art. no. 012032.